Palaeogeography, Palaeoclimatology, Palaeoecology 350–352 (2012) 180–188

Contents lists available at SciVerse ScienceDirect

Palaeogeography, Palaeoclimatology, Palaeoecology

journal homepage: www.elsevier.com/locate/palaeo

Extinction patterns, δ^{18}O trends, and magnetostratigraphy from a southern high-latitude Cretaceous–Paleogene section: Links with Deccan volcanism

Thomas S. Tobin [a,*], Peter D. Ward [a], Eric J. Steig [a], Eduardo B. Olivero [b], Isaac A. Hilburn [c], Ross N. Mitchell [d], Matthew R. Diamond [c], Timothy D. Raub [e], Joseph L. Kirschvink [c]

[a] University of Washington, Earth and Space Sciences, Box 351310, Seattle WA 98195, United States
[b] CADIC-CONICET, Bernardo Houssay, V9410CAB, Ushuaia, Tierra del Fuego, Argentina
[c] California Institute of Technology, Geological and Planetary Sciences, 1200 E. California Blvd. Pasadena CA 91125, United States
[d] Yale University, Geology & Geophysics, 230 Whitney Ave. New Haven, CT 06511, United States
[e] University of St. Andrews, Department of Earth Sciences, St. Andrews KY16 9AL, UK

ARTICLE INFO

Article history:
Received 19 April 2012
Received in revised form 27 May 2012
Accepted 8 June 2012
Available online 10 July 2012

Keywords:
Mass extinction
K–Pg
Paleotemperature
Magnetostratigraphy
Antarctica
Deccan Traps

ABSTRACT

Although abundant evidence now exists for a massive bolide impact coincident with the Cretaceous–Paleogene (K–Pg) mass extinction event (~65.5 Ma), the relative importance of this impact as an extinction mechanism is still the subject of debate. On Seymour Island, Antarctic Peninsula, the López de Bertodano Formation yields one of the most expanded K–Pg boundary sections known. Using a new chronology from magnetostratigraphy, and isotopic data from carbonate-secreting macrofauna, we present a high-resolution, high-latitude paleotemperature record spanning this time interval. We find two prominent warming events synchronous with the three main phases of Deccan Traps flood volcanism, and the onset of the second is contemporaneous with a local extinction that pre-dates the bolide impact. What has been termed the K–Pg extinction is potentially the sum of multiple, independent events, at least at high latitudes.

1. Introduction

Five major mass extinction events punctuate the history of animal life on earth. Of these, the Cretaceous–Paleogene (K–Pg) extinction is the most recent and well-studied. Like all mass extinctions, the K–Pg event was originally interpreted as a gradual event, but the discovery of unmistakable evidence of a large bolide impact with the Earth essentially coincident with the paleontologically recognized K–Pg mass extinction (Alvarez et al., 1980) led to a change in this paradigm. Today, more than three decades since the Alvarez et al. (1980) publication, a large number of researchers are convinced that the bolide impact, located near present day Chicxulub, Mexico (Hildebrand et al., 1991), was either solely or largely responsible for the K–Pg extinction (Schulte et al., 2010). This view, however, has never been universal (Archibald et al., 2010; Courtillot and Fluteau, 2010), and reported evidence for impacts at the late Devonian (Playford et al., 1984), end Permian (Becker et al., 2001), and end Triassic extinctions (Olsen et al., 2002) have been disputed (respectively, McLaren, 1985; Farley et al., 2005; Tanner et al., 2008). Another candidate that may cause mass extinction, flood basalt volcanism, has been claimed to demonstrate strong temporal correlation with all mass extinction events over the past ~360 Ma, including the Deccan Traps large igneous province at the K–Pg boundary (Alvarez, 2003; Courtillot and Renne, 2003). Global warming, with associated climatic complications, provides a likely causal link between flood volcanic episodes at the Permian–Triassic (Siberian Traps) and Triassic–Jurassic (Central Atlantic Magmatic Province—CAMP) mass extinctions (Kump et al., 2005; Whiteside et al., 2010). Another hypothesis suggests that both flood volcanism and bolide impact combined are necessary for a major mass extinction (White and Saunders, 2005; Arens and West, 2008).

If flood basalt volcanism on a scale equivalent to the Siberian Traps or CAMP was indeed a mechanism causing mass extinction of species, there should be some signature of this during the emplacement of the Deccan Traps. To date, the geologically short interval during which the extinction, volcanism, and the impact occurred has confounded efforts to separate the biotic effects of Deccan Traps volcanism and the Chicxulub impact on end Cretaceous extinctions. The Deccan Traps erupted in three discrete pulses (Chenet et al., 2009; Jay et al., 2009), the second of which extruded a volume of basalt comparable to the Siberian Traps or CAMP events (Courtillot and Renne, 2003) sometime during the 400 kyr prior to the K–Pg boundary. The outcrop sections on Seymour Island, Antarctica, provide an ideal place to examine the biotic impacts of Deccan volcanism due to their expanded nature and high paleolatitude location, allowing high temporal resolution in a location with increased sensitivity to climate change.

* Corresponding author. Tel.: +1 813 545 1912.
E-mail address: ttobin@u.washington.edu (T.S. Tobin).

0031-0182/$ – see front matter © 2012 Elsevier B.V. All rights reserved.
doi:10.1016/j.palaeo.2012.06.029

2. Field setting

Seymour Island is located off the northeast of the Antarctic Peninsula (Fig. 1) at 64°S. It contains the stratigraphically highest exposures in the James Ross Island Group, well-exposed back-arc basin marine deposits that span the Early Cretaceous through the Early Paleogene. The basin has experienced minimal tectonic modification in the past 80 Ma, as evidenced by minor homoclinal tilt (5°–9°) and well-preserved fossils. Reconstructed paleolatitude (62°) is similar to current latitude and is in agreement with plate reconstructions (Torsvik et al., 2008), making Seymour Island one of the highest-paleolatitude K–Pg boundary outcrops. This location makes it ideal for examining climate changes associated with the K–Pg extinction, since polar amplification is likely to produce larger and more detectable temperature changes at high latitudes (Manabe and Stouffer, 1980; Holland and Bitz, 2003).

On Seymour Island, the biostratigraphically determined Maastrichtian through lower Danian interval is represented by the López de Bertodano Formation (LBF) which is uncomformably overlain by the Sobral Formation of Paleocene age. The LBF is comprised of over 1000 m of predominantly immature mudstones with interspersed sandy and concretionary layers. Ten numbered informal lithostratigraphic units have been defined (Macellari, 1986, 1988) and are used here. This study focuses on the upper "molluscan units" (Units 7–10), which become increasingly fossiliferous through Units 9 and 10. Comprised mostly of siltstones with a larger percentage of sand and concretionary layers than the lower units, these upper units are interpreted as transgressive over the lower group, deposited in shelf and slope facies at water depths between 100 and 200 m (Macellari, 1988; Olivero, 2012). Horizons containing early-diagenetic carbonate concretions, often rich in fossils, occur throughout at roughly ten-meter intervals. Although modern freeze-thaw cycling can disturb the structural integrity of finer-grained and loosely-consolidated mudstones, many of these indurated concretions retain their original orientation with respect to bedding and are suitable for paleomagnetic analysis.

Most fossils exhibit outstanding preservational characteristics, including the primary mineralogy and undeformed three-dimensional shape. Most mollusks, with the exception of originally calcitic pycnodonte bivalves, preserve original aragonite, which is recrystallized easily by heating or any form of diagenesis. Its presence is used as a guide for the collection of paleomagnetic and geochemical samples with minimal levels of thermochemical alteration (Filmer and Kirschvink, 1989; Ward et al., 1997).

The K–Pg boundary has been located between Units 9 and 10 of the upper LBF through various means in the past and is currently defined by the first occurrence of Paleogene dinocyst fossils that are essentially coincident with an iridium enhancement (Elliot et al., 1994). Apart from the iridium anomaly, global correlation of the late Cretaceous interval on Seymour Island has been hampered by the increasing endemism of macrofossils and microfossils in the Maastrichtian (Macellari, 1987; Olivero and Medina, 2000; Bowman et al., 2012) and an absence of any absolute age control from ash layers. While some age constraints from Sr isotope ratios on molluscan carbonate have been reported from the lower units of the LBF (McArthur et al., 2000), no age constraints prior to this study have been reported from the youngest units of this formation that approach and cross the K–Pg boundary.

3. Methods

The results of this paper hinge on three separate analytical techniques which are detailed below. Fossil material and paleomagnetic samples were collected from stratigraphic sections largely following previous studies (Macellari, 1988; Crame et al., 2004; Olivero et al., 2007). A schematic sample path is mapped in Fig. 1, and specific GPS coordinates are available in Table S1. Magnetostratigraphy was used to create a high resolution chronostratigraphic framework that allows for global correlation. Oxygen isotope analysis of well preserved fossil shell carbonate was used to reconstruct sea water temperature over the same stratigraphic interval. Additionally, fossil occurrence data from previous studies (Zinsmeister et al., 1989) were reexamined using modern statistical techniques that place confidence intervals on local multi-species extinctions (Wang and Marshall, 2004).

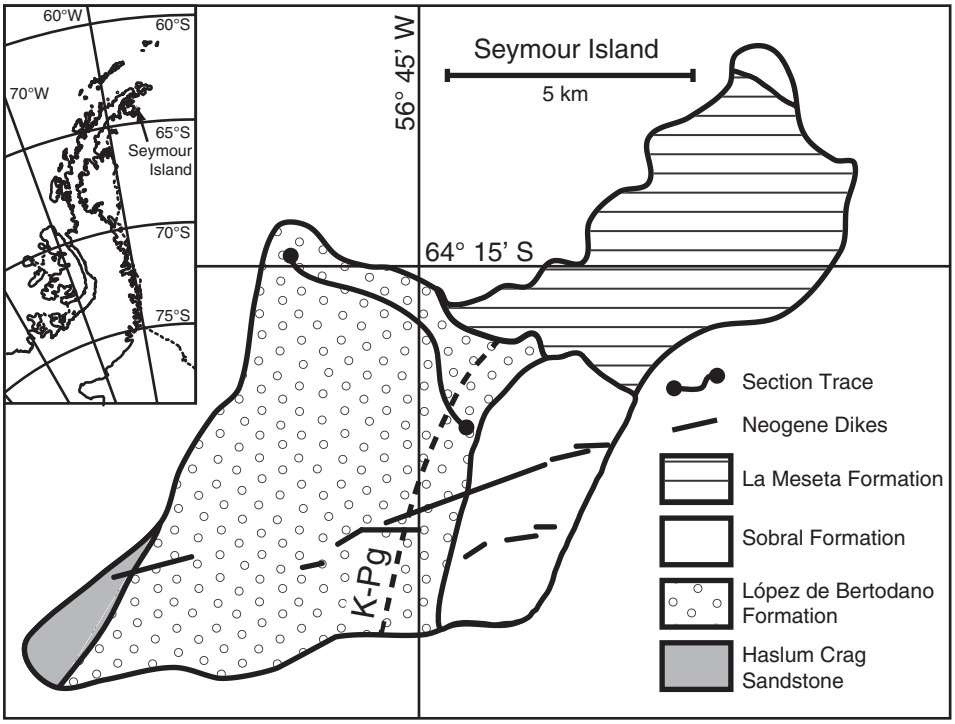

Fig. 1. Map of Seymour Island and its location on the Antarctic Peninsula (inset) showing location of geologic formations and sampling trace, adapted from Dutton et al. (2007). GPS coordinates for sampling trace are available in Table S1.

3.1. Paleomagnetism and magnetostratigraphy

On Seymour Island, the LBF has deterred previous paleomagnetic studies primarily due to the tendency of the mudstone matrix to become unconsolidated during annual freeze-thaw cycles. It was thought that this annual surface disruption would scramble the orientation of any magnetic particles capable of preserving a stable natural remanent magnetization (NRM). However, the formation contains numerous layers with early-diagenetic carbonate-cemented concretions that are demonstrably in place; many of these contain 3-dimensionally preserved macrofossils, implying that the cementation occurred during early diagenesis before sedimentary compaction. Such concretions are thought to form by initial carbonate cementation at grain-grain contacts, a process that acts to lock in post-depositional remanent magnetizations without the inclination errors associated with sediment compaction (Filmer and Kirschvink, 1989; Ward et al., 1997). We targeted these concretionary horizons preferentially for paleomagnetic analysis. GPS coordinates for these major concretion beds, as well as their tie-in to the measured stratigraphic section, are given in Table S1. Digital images of sampling sites, as well as the magnetic data used in this study, are deposited at the Magnetic Information Consortium (MagIC) site (http://earthref.org/MAGIC/).

Thermochemical alteration is essentially absent in the Campanian through Maastrichtian strata of the James Ross Basin. Molluscan fossils from Seymour Island preserve nacreous metastable aragonite. Iridescence in molluscan nacre is a result of a diffraction grating effect of un-denatured protein layers within the original aragonite (Lowenstam and Weiner, 1989), and its presence in ancient rock constrains the peak burial metamorphic conditions to be less than ~60 °C with none of the thermochemical alteration which often remagnetizes sediments. In addition, extensive petrographic work reported by Pirrie (1994) shows no evidence for smectite–illite transformation, conversion of clinoptilolite–heulandite to analcite, increased vitrinite reflectivity, or resetting of fission-tracks in apatite, all of which are consistent with shallow burial and no significant heating. Presumably, secondary magnetic components would be due to a combination of viscous remanent magnetizations (VRMs) or the formation of antiferromagnetic minerals during recent surface weathering. However, in sediments of this sort it is quite common for thermochemical changes during demagnetization at fairly low temperatures (<300 °C) to produce fine-grained ferrimagnetic phases during decomposition of clays and Fe-rich carbonate phases. Hence, it is necessary to use the hybrid demagnetization strategies noted below to identify and isolate secondary components, and much of the stable remanence appears to be preserved in ferrimagnetic minerals (such as biogenic magnetites) that have blocking temperatures <300 °C due to thermal-demagnetization reactions. These techniques have proven effective in past studies of Cretaceous sediments with similar lithologies (Filmer and Kirschvink, 1989; Ward et al., 1997).

We collected samples for paleomagnetic analysis as oriented blocks broken from concretions that were judged to be essentially in place (examples in Figure S1). As surface weathering can produce a trace of the antiferromagnetic mineral goethite, we took special care to crack open concretions in the field in search of those that were visibly the least altered. From these we cut a series of 1 cm-high, 2.54 cm diameter cylindrical samples for paleomagnetic and rock magnetic analyses. One or more specimen from each sample was analyzed at the California Institute of Technology paleomagnetics laboratory, using 3-axis DC-SQUID moment magnetometer systems housed in magnetically shielded rooms. The background noise of these instruments is less than 1 picoA·m^2, and they are equipped with the vacuum pick-and-place, computer-controlled sample handling systems that can measure up to 180 samples automatically. AF demagnetization was performed with computer-controlled, three-axis coil systems fit in-line in the sample path. Thermal demagnetization was performed in commercially-built magnetically shielded furnaces that had been modified to minimize sample oxidation by using a gentle flow of N_2 gas to expel air and measured twice after each set of demagnetization experiments, in the 'arrow-up' and 'arrow-down' modes (Kirschvink et al., 2008). This allows the averaging of eight sets of independent measurements, providing several additional measures of measurement reliability.

For paleomagnetic analyses, one sample was selected for detailed demagnetization from the sample set generated at each locality, and if this proved to unstably magnetized, additional sub-samples were run through the demagnetization analysis, particularly from sites in critical intervals. Specimens were initially measured for NRM and then subjected to several low-temperature cooling cycles in liquid nitrogen (77°K) to remove viscous components often held by magnetically-soft, multi-domain magnetite grains that might be present (Halgedahl, 1993; Dunlop and Ozdemir, 1997). This was then followed by low alternating-field (AF) demagnetization up to 6.9 mT in 2.3 mT steps to remove low coercivity magnetizations, such as those that might have been introduced during passage through airport X-ray machines. The samples were then treated with thermal demagnetization from ~60 °C in 5 to 25 °C increments up to 400 °C, or until they displayed unstable, irreproducible behavior (examples shown in Fig. S2), presumably from the formation of magnetite from thermal decomposition of glauconitic clays. Demagnetization data were analyzed using principal component analysis (Kirschvink, 1980), using the now-standard criteria: Only demagnetization lines with MAD values below 10° and circles below 15° were included in the statistical analysis shown in Fig. 2 and Table 1. Mean directions were obtained using Fisher statistics (Fisher, 1953). The method of McFadden and McElhinny (1988) was used for combining data from demagnetization lines and arcs, and the final iterative directions along the arc constraints were combined with lines for the stratigraphic polarity interpretation. The reversals test followed that of McFadden and McElhinny (1990).

3.2. Rock magnetism

A series of rock-magnetic analyses were also performed on representative samples of each lithology, using routines implemented on the RAPID consortium magnetometers (Kirschvink et al., 2008). The NRM of these specimens was demagnetized in 3-axis alternating fields in 21 logarithmically distributed steps between 2.1 and 80 mT. This was followed by a 20-step progressive ARM acquisition in 100 mT AF fields along the vertical axis with a DC biasing field between 0 and 1 mT. The maximum ARM was then AF demagnetized in the same logarithmic sequence used on the NRM, except along the vertical axis only and up to the maximum vertical AF field of 158.4 mT (28 steps). The sample was then given a vertical-axis IRM of 100 mT and AF demagnetized in the same 28 steps. An IRM acquisition series was then run with the same logarithmic sequence, but up to the maximum IRM pulse field of 350 mT (36 steps). In turn, this saturation IRM was AF demagnetized in the 28 step sequence up to 158.4 mT. Finally, the sample was given an IRM of 350 mT, the polarity of the pulse was reversed, and it was subjected to a 36-step DC backfield demagnetization. This set of experiments allows the construction of moderately high-resolution coercivity spectra, as well as the determination of parameters, including IRM and ARM strength, coercivity of remanence, the Cisowski (1981) magnetostatic interaction parameter R, and ARM susceptibility. This total ~200-step experiment takes ~4.5 h per specimen. MATLAB scripts used to analyze the rock magnetic data are available through links on the RAPID website (www.rapid.gps.caltech.edu).

3.3. Paleotemperature

Fossil shell carbonate from ammonites, gastropods, bivalves and echinoids was collected for isotopic analysis of $\delta^{13}C$ and $\delta^{18}O$. Carbonate material was powdered using a Merchantek Micromill for precise sampling of shell material. Powdered material was analyzed using a Kiel III Carbonate Device attached to a Delta Plus isotope ratio mass

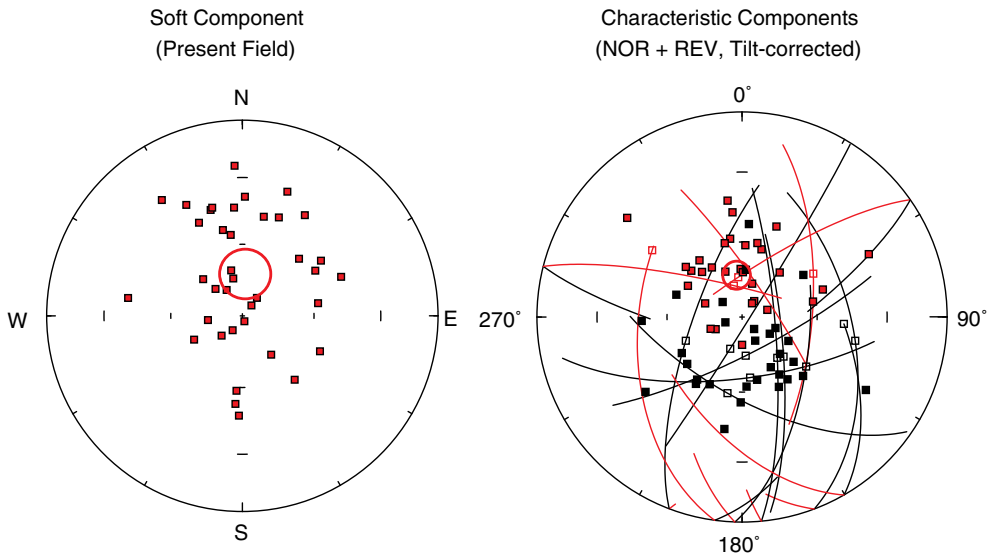

Fig. 2. Equal-area plots showing the principal magnetic components isolated from the demagnetization data generated in this study. Directions obtained from linear components are shown as solid squares, and the arc-segments show the constraints from demagnetization planes (McFadden and McElhinny, 1988) with the last directional iteration indicated as a hollow square. Data for the cones of 95% confidence are shown in Table 1. Black (red) points are lower (upper) hemisphere.

spectrometer. Samples (0.020–0.100 mg) were reacted at 70 °C with 100% anhydrous phosphoric acid and analyzed interspersed with internal lab calcite standards calibrated to NBS-18 (−23.01‰ VPBD) and NBS-19 (−2.20‰ VPDB) for $\delta^{18}O$ and NBS-19 (+1.95‰ VPBD) and LSVEC (−46.6‰ VPBD) for $\delta^{13}C$. Fractionation factors for aragonite and calcite at 70 °C follow Kim et al. (2007a).

Despite surface confirmation of visibly unaltered material in thick section, the process of drilling into a sample may still entrain adjacent, altered material. The powder aliquot from each sample was analyzed for trace element concentrations, including Fe, Mg, Mn, Sr, and Na, using an ICP-AES. These data were used to assess diagenesis, both through comparison with published ranges of accepted, unaltered values (Morrison and Brand, 1986; Brand and Morrison, 1987) and through comparison with the $\delta^{18}O$ data. Representative samples of aragonite fossil species common in the section were analyzed using X-Ray Diffraction (XRD) to confirm both primary mineralogy and diagenesis. All analyzed molluscan samples, with the exception of pycnodonte (calcite-secreting) bivalves, were confirmed as aragonite with no detectable calcite present.

The $\delta^{18}O$ values in their stratigraphic context divided taxonomically can be seen in Fig. 3. Each taxonomic group was analyzed for covariance between $\delta^{18}O$ and concentration of Fe, Mg, Mn, Sr, and Na and compared with accepted ranges (example in Fig. S3). As many as half of all shells (n = 168) were found to be higher than the thresholds for Fe (within limits n = 83) and Mn (n = 91), a third for Mg (n = 127), and a fifth for Sr (n = 149) and Na (n = 139). Culling the data by removing shells outside the limits for each trace element does not alter the overall $\delta^{18}O$ pattern. Similarly, the $\delta^{18}O$ patterns for each taxonomic group analyzed individually are largely indistinguishable from the whole data set provided stratigraphic coverage was sufficient (e.g. echinoids have little stratigraphic coverage and ammonites are not found in the Danian). Cross plots of $\delta^{13}C$ v. $\delta^{18}O$ showed no significant statistical trends for any taxonomic group (Fig. S4). Values of r^2 ranged from .26 (gastropods) to .009 (bivalves). Though there were large variations in $\delta^{13}C$ for echinoids and ammonites, removal of shells with "anomalous" $\delta^{13}C$ values from the data set had no significant effect on reconstructed paleotemperature patterns. Due to the lack of significant covariance between any individual trace element and $\delta^{18}O$ for any taxonomic group and the similarities between all versions of the culled data and the full data set, we reconstructed the paleotemperature record using the full data set, though the data set culled based on trace element concentrations is also displayed.

Paleotemperature estimates were made following the procedures of Kim et al. (2007b) and Kim and O'Neil (1997) for aragonite and calcite respectively. Organisms generally deposit carbonate under equilibrium conditions with respect to seawater (Weiner and Dove, 2003). For the Cretaceous, this seawater is assumed to be −1.0‰ (VSMOW) based on modeled ocean chemistry given a predominantly ice-free world (Shackleton and Kennett, 1975). The paleotemperature record through the section was created by taking the mean of multiple measurements on each shell, and then taking the mean of all averaged shell values in 100 kyr bins (see Section 4.3). Uncertainties are reported as 1.96× standard error, equivalent to a 95% confidence interval (Altman and Bland, 2005). The uncertainties for time bins containing only a single shell were omitted, as the standard deviation could only be calculated for intra-shell variation, a significant underestimation of the uncertainty.

Table 1
Paleomagnetic results from Units 5–10 of the López de Bertodano Formation on Seymour Island, Antarctic Peninsula. 'N_{eff}' indicates the effective number of samples in the analysis, and numbers indicated like '(L, C)' give the number of individual demagnetization Lines and Circles, respectively (N_{eff} = L + ½P (McFadden and McElhinny, 1988)). NOR = Normal, REV = Reversed magnetic field direction; PLF = Present local field. R = mean resultant vector length; α95 = radius of 95% confidence cone around mean; κ = Fisher precision parameter (Fisher, 1953). dp, dm = confidence limits on pole for semiminor/semimajor axes respectively. G_r = Fisher test statistic.

LBF Units 5–10, Seymour Island, summary of Fisherian statistics

	N (eff.)	R	Decl.	Incl.	α95	κ
NOR + REV	67.5 (60, 15)	61.5	27.8	−77.1	5.45°	11.04
	tilt corr:	61.5	352.5	−73.1	5.45°	11.03
NOR	32 (30, 4)	29.6	27.8	−74.7	7.31°	13.07
	tilt corr:	29.6	356.9	−71.1	7.31°	13.05
REV	35.5 (30, 11)	31.9	208.1	79.6	8.21°	9.58
	tilt corr:	31.9	166.9	75.0	8.20°	9.59
PLF	38	31.8	4.2	−72.5	10.43°	5.94

The combined tilt-corrected pole is at 83.3° N, 267.5° E, (dp, dm) = (9.8°, 10.7°), paleolatitude −62° ± 9°.
The hypothesis that the Normal and Reversed directions are antiparallel cannot be rejected at the 95% confidence level (Gr = 1.23, Chi^2, p. value 0.542), passing the McFadden and McElhinny reversal test in category "C" (Antiparallel angle = 4.9°; Critical angle = 10.7°).

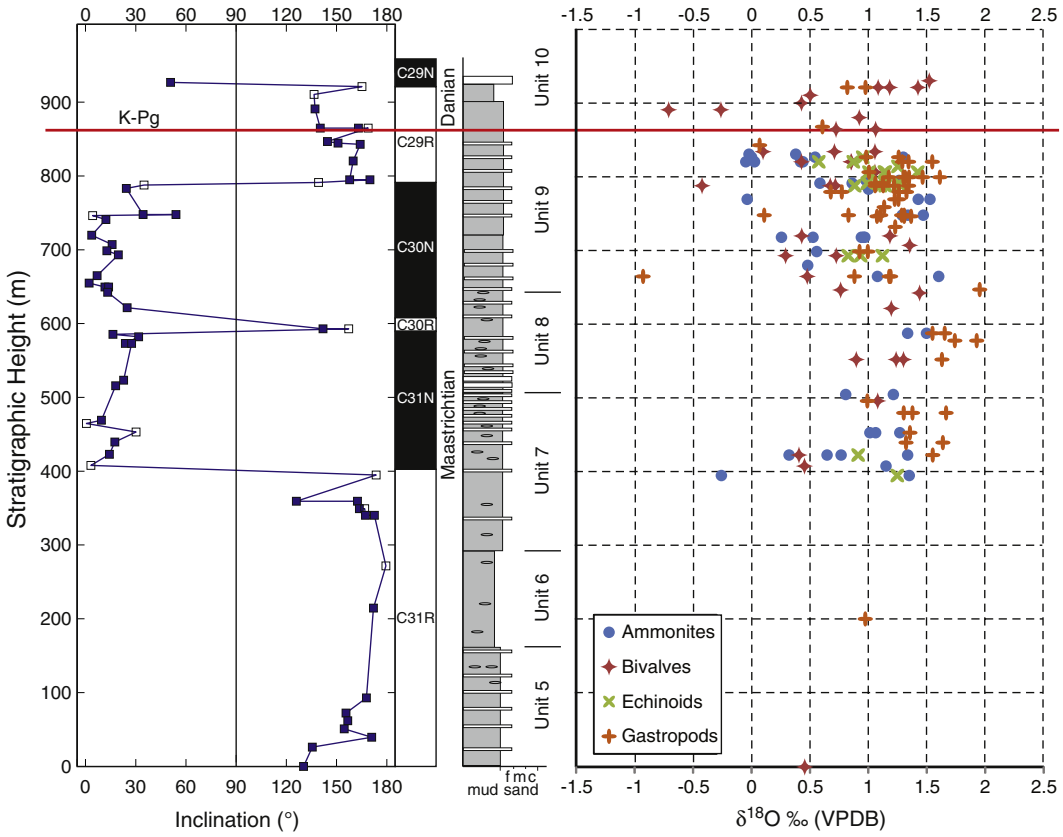

Fig. 3. Compiled magneto-, litho-, and isotopic stratigraphic results for the upper half of the Lopéz de Bertodano Formation, representing the Maastrichtian and Lower Danian interval. Units are the informal units as described by Macellari (1986). At left is the magnetic polarity interpretation is indicated by the tilt-corrected inclination of the stable remanence vectors, with solid symbols indicating results from samples that demagnetize to a stable end position and open symbols showing the final iterative position of best directions along the demagnetization arcs. At right are the $\delta^{18}O$ values sorted by major taxonomic group.

3.4. Extinctions

The molluscan units of the LBF contain a diverse array of invertebrate fauna and a smaller number of marine reptiles and other vertebrates. We analyzed 326 occurrences distributed among 77 species from Units 8–10 previously reported from Seymour Island (Zinsmeister et al., 1989). For a quantitative analysis of extinction patterns, we eliminated fauna with only one stratigraphic occurrence. The technique for assigning a confidence interval to an extinction event was first undertaken by Marshall (1995) in this locality using only ammonite species. Here we increase the sample size by utilizing other, largely molluscan, taxonomic groups as well. Extinction confidence intervals were calculated using the methods of Wang and Marshall (2004). We diverged from their methods in calculating confidence intervals without one of their recommended improvements to Marshall (1995), as we did not use the highest stratigraphic occurrence of any of the included species as the lower bound of the extinction confidence interval. By employing this method, we could better test whether different extinction events were stratigraphically distinct.

4. Results

4.1. Rock magnetism results

Results support the interpretation that the NRM is carried by fine-grained magnetite of detrital origin, although some antiferromagnetic minerals from weathering might also be involved. Rock magnetic data from a suite of six representative samples are summarized in Figure S5. In particular, the Lowrie–Fuller test on all samples is strongly positive, indicating the magnetic mineralogy of particles with Hc values below 100 mT is dominated by interacting single-domain to pseudo-single-domain behavior. Similarly, ARM acquisition characteristics indicate dominance by strongly interacting pseudo-single-domain to multi-domain particles. However, the median destructive field of IRM acquisition tends to be about 80 to 100 mT, arguing against a large multi-domain magnetite fraction, indicating that the PSD particles must be fairly elongate. This is in agreement with the liquid nitrogen cycling, which typically would unblock only 5–20% of the NRM. Less than 5% of the IRM is gained in fields above 300 mT, suggesting a minor fraction perhaps from antiferromagnetic minerals that typically are present from surface weathering. The Fuller test of NRM origin in all cases shows that the ARM values upon demagnetization are two to three orders of magnitude greater than the values of the NRM, which strongly suggests that the NRM is either detrital or chemical in nature.

4.2. Paleomagnetism and magnetostratigraphy results

Slightly over half of the paleomagnetic samples (63/112) could be characterized as well behaved, with most having at least one specimen which possessed a component of low AF and thermal stability similar to the present magnetic field direction in Antarctica, as well as one or two additional components of higher stability. Due to the overall shallow dip of the beds on Seymour Island and the similarity of the Late Cretaceous paleogeography for Antarctica to that of the recent, the Reversed characteristic directions (South and Down) are easy to separate from modern-day overprints (North and Up). However, Normal samples are difficult to distinguish from samples with strong recent overprints without using some other objective criteria.

On the assumption that the intrinsic polarity of a sample does not depend on the magnetic mineralogy, we first analyzed the stability spectra of samples displaying Reversed components as a guide to the stability spectra of both the Normal and Reversed characteristic components. A Normal polarity interpretation therefore required demagnetization stability well into that displayed by the group of Reversely magnetized samples, aided sometimes by the presence of short great-circle arcs at the low demagnetization ends.

Representative orthogonal projections of the demagnetization trajectories are shown in Fig. S2, and all of the demagnetization data used for this paper are deposited in the Magnetic Information Consortium (MagIC) database. Below about 250 to 300 °C, demagnetization trajectories generally are stable and linear, giving the character of the underlying characteristic component. Above these values, however, magnetic directions often become erratic, apparently picking up spurious directions even in the weak magnetic field (<200 nT) of the shielded laboratory room. Monitoring of the remanence with susceptibility before each measurement suggests that we are experiencing the decomposition of iron bearing clays, and perhaps some of the pyrite, into finer-grained ferrimagnetic minerals. Nevertheless, the removal of multi-domain magnetite carriers with low temperature cycling in liquid nitrogen, followed by low-field alternating field demagnetization, and the fact that the rocks have never been heated appreciably above even 60 °C, argue that we are seeing a real characteristic component of Cretaceous age before the samples become unstable. As noted below, we also find that the magnetic polarity of this characteristic component is in broad agreement with the geomagnetic reversal timescale for late Maastrichtian and early Danian time.

As a group, the mean normal and reversely magnetized directions isolated with this procedure are statistically anti-parallel, passing the reversals test (mean angular offset 4.9°, critical angle 10.7°, see Table 1) for a Category C of McFadden and McElhinny (1990). The combination of the positive reversals test and the presence of layer-bound magnetic polarity zones strongly imply that the characteristic magnetization was acquired at or shortly after the time of deposition. Given the robust number of samples yielding useable results and the excellent age constraints on the K–Pg boundary, the mean direction rates a perfect 7 on the 7-point paleomagnetic quality (Q) index of Van der Voo (1993).

The magnetostratigraphic record for the Maastrichtian through lower Danian on Seymour Island is shown in Fig. 3. All sites from the oldest part of the sequence, Units 5, 6, and those at the bottom of 7, are reversely magnetized, whereas the upper half of Unit 7, most of 8, and the lower half of 9 are Normal. A short Reversed interval is characterized by two samples in the middle of Unit 8, and the upper half of Unit 9 and most of Unit 10 are Reversed. One Normal sample was measured at the top of Unit 10 prior to the overlying unconformity. This magnetic polarity pattern has a straightforward interpretation. The K–Pg boundary is known to occur within Magnetic Chron 29R (Alvarez et al., 1977), which identifies the Reversed zone in the top half of Unit 9, and most of Unit 10, as C29R. The reversed interval in Unit 8 is most likely the short duration C30R, while the overlying and underlying Normal zones are C30N and C31N respectively. The lowest zone is C31R, though its base is unconstrained. The uppermost point in Unit 10 is likely the beginning of C29N. A chronostratigraphic framework (Fig. 4) was constructed with linear interpolation between the known time points provided by these reversals and the K–Pg boundary (Gradstein et al., 2004) adopted here. The consistent sedimentation rate through the section further supports the above magnetostratigraphic interpretation.

4.3. Paleotemperature results

Shown in Fig. 5 is the paleotemperature record in 100 ka binned intervals using an age model described above (Section 4.2). Data from all analyzed specimens, as well as a culled selection based on diagenetic indicators, are both shown and largely consistent (see Section 3.3). Overall, these paleotemperature results are consistent with previous macrofossil studies in this area (Ditchfield et al., 1994; Elorza et al., 2001; Dutton et al., 2007) as well as estimates from microfossils (Barrera et al., 1987), when analyzed using newly available calibrations for carbonate-temperature (Kim et al., 2007b) and carbonate-acid (Kim et al., 2007a) relationships. Warming intervals are highlighted during any continuous warming trend of at least 3 °C, excluding data points comprised of a single shell, yielding two notable warming events. The first occurs between 67.9 and 67.1 Ma, the second between 65.8 and 65.3 Ma. The second warming interval could plausibly be split into two separate events 65.8–65.6 Ma and 65.5–65.3 Ma, an interpretation supported by the culled data set. The difference between these two intepretations is primarily seen in the magnitude of the warming and the decay rate of the climatic perturbation. Both possibilities are explored in a statistical analysis in Section 5. Warming during the last several thousand years of the Cretaceous has been recognized in deep ocean cores from benthic foraminiferal data at both mid- (Li and Keller, 1998) and southern high latitudes (Barrera, 1994; Barrera and Savin, 1999), though at lower magnitudes. Similar patterns have also been observed in mid-latitude terrestrial and near-shore settings (Wilf et al., 2003), suggesting that temperature variability at high latitudes may reflect change on a global level.

4.4. Extinction results

Fig. 6 shows previously reported faunal data from the LBF and newly determined extinction confidence intervals, demonstrating two separate extinction events. Species with a single occurrence are included in the figure but not in the statistical evaluation. The latter of the two extinctions is synchronous with the K–Pg boundary, while the earlier occurs over a narrow interval 40 m below the K–Pg. Using the age model described in Section 4.3, this event occurs approximately 150 kyr prior to the K–Pg boundary. There is a notable difference in the selectivity of the two extinctions relative to the organisms' mode of life. The precursor extinction affects 10 marine invertebrate species, 9 of which are benthic, in contrast to the K–Pg boundary extinction where only 6 of 14 total extinct species are benthic. There is no apparent selectivity to the extinction within benthic fauna relative to trophic level or sediment position in the precursor extinction. The most striking difference between these two extinctions is apparent in the fate of ammonites: only one of seven ammonites becomes extinct at the precursor extinction, whereas all six ammonites present in the latest Maastrichtian become extinct at the K–Pg boundary.

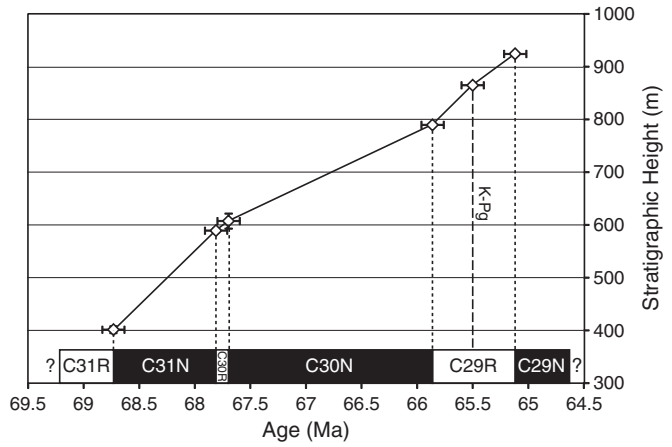

Fig. 4. Age model assuming constant sedimentation rate between known tie points derived from magnetostratigraphy and the K–Pg boundary. Sedimentation rate is fairly constant throughout the interval (0.1–0.2 mm/a).

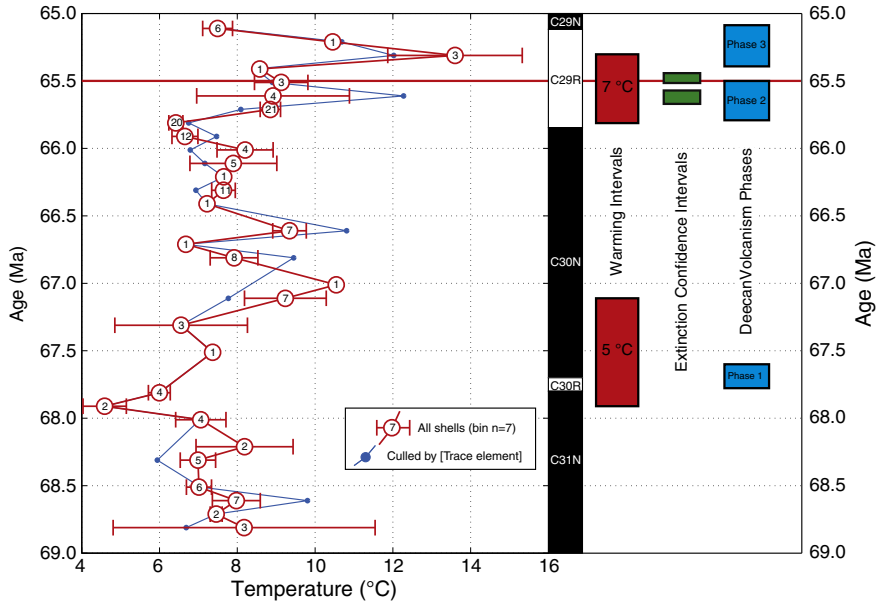

Fig. 5. Reconstructed paleotemperature record from $\delta^{18}O$ in molluscan shell carbonate using all shells (open circles) and a culled data set where shells outside trace element bounds are not included (in blue, see Section 3.3). Data is binned in equal time bins of 100 ka, with uncertainties representing a 95% confidence interval (standard error × 1.96 (Altman and Bland, 2005)) based on multiple shells, while the circled number represents the number of shells in a given bin. Warming intervals of greater than 3 °C are highlighted. At right are the extinction intervals observed in Fig. 4, as well as the magnetostratigraphically correlated phases of Deccan Traps flood volcanism. Correlations between warming and volcanism are statistically significant ($p<0.01$, see Section 5).

While the precursor extinction event is visible in Fig. 6, there is a notable lack of fossil collection in the interval between the two extinction events, and the earliest extinction could plausibly be explained by artificial range terminations due to poor sampling. To test this observation, extensive collections were made during recent sampling expeditions. New fossil occurrences ($n=634$) were recorded and combined with species occurrences from Zinsmeister using the well-defined K–Pg boundary as a datum. While relative stratigraphic heights are well determined for a single data set (hence Fig. 6 showing the Zinsmeister data alone), correlating two separate sections necessarily generates greater uncertainty in both species identification and stratigraphic height, particularly at greater stratigraphic distances from the K–Pg datum. Consequently, new species occurrences were only added if they were separated by greater

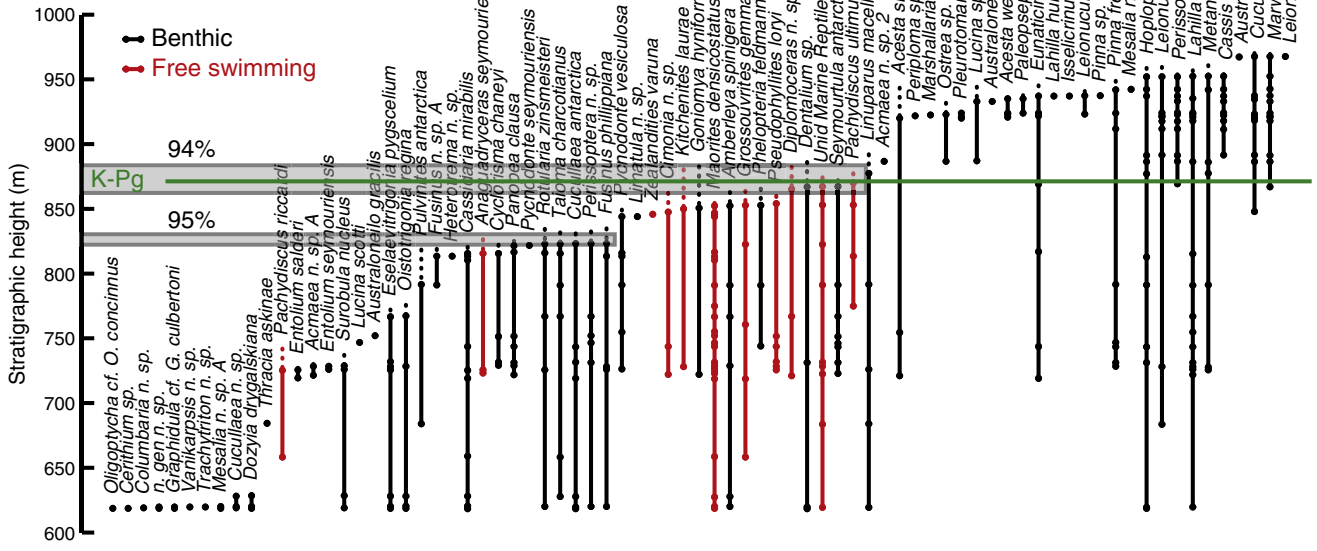

Fig. 6. Faunal range data from Zinsmeister et al. (1989) reevaluated using modern extinction confidence interval analysis (Wang and Marshall, 2004). Individual species extinction confidence intervals (those used in the multi-species extinction analysis) are shown as dashed range extensions. Grey bars highlight multi-species extinction confidence intervals. Two extinction events were discovered to be stratigraphically resolvable, one at and one prior to the K–Pg boundary. Species with single occurrences pictured above are omitted from statistical analyses.

than twenty meters stratigraphically, a very conservative approach. Several species have been renamed or combined in the past twenty years, and these changes also incorporated in the combined analysis and figure (Fig. S6), demonstrating the persistence of two multi-species extinction events despite thorough sampling over the previously barren interval.

5. Discussion

Fig. 5 places the observed extinctions and paleotemperature record in their stratigraphic context, along with the timing of Deccan Traps flood volcanism as correlated using magnetostratigraphy (Chenet et al., 2009; Jay et al., 2009; Robinson et al., 2009). This framework reveals that warming intervals occur primarily during the phases of Deccan Traps volcanism, and the onset of the second interval is also contemporaneous with the identified precursor extinction. As discussed in Section 4.3, the later warming event could be subdivided into two events corresponding with the two latest Deccan Traps phases. Below we evaluate both possibilities and find that both interpretations yield similar correlation coefficients.

A statistical evaluation of correlation between warming events and the timing of Deccan volcanism was performed by assigning binary values to the two variables at 100 ka intervals throughout the section as in Fig. 5, from 68.8 Ma to 65 Ma. Each variable was assigned a value of 1 if 'active' and 0 if 'inactive' for each 100 ka interval. The timing of warming events and volcanic phases correlate with a phi correlation coefficient (φ) of 0.45, indicative of a moderately strong correlation with high statistical significance (p-value<0.01). The correlation is similar ($\varphi = 0.39$; $p<0.03$) if the diagenetically culled data set is evaluated. We were unable to perform this analysis on the extinction timing due to a lack of fossil data during the earliest warming period.

The integration of the first Upper Cretaceous magnetostratigraphy for this basin with the high resolution temperature record presented here reveals a significant destabilization in polar climate in the Late Maastrichtian caused by global warming, likely the result of Deccan volcanism. This supports the hypothesis that the primary long term effect of LIP emplacement is a global warming as a consequence of CO_2 outgassing (Wignall, 2001). Furthermore, correspondence between multi-species extinction and warming strengthen the proposed causal link between flood basalts and biotic crises (Courtillot and Renne, 2003).

6. Conclusion

Climatic effects on biota occur rapidly on a geologic time scale and may only be discernible in expanded sections such as those found in the James Ross Basin. In more condensed sections elsewhere, such a precursor extinction may be time-averaged with, and indistinguishable from, the boundary extinction. The preferential extinction of benthic fauna compared to nektic species during the precursor extinction, compared with primarily nektic extinction (including all ammonites) at the K–Pg boundary extinction, suggests that substantially different mechanisms were at work in each event. Our results imply that what has been called the K–Pg mass extinction was composed of a more complicated series of separate events than any single cause can explain. Furthermore, the lack of biotic response to Deccan volcanism has been used as a reason to reject the hypothesis that large igneous provinces significantly disrupted the biosphere during the end Triassic (CAMP) and end Permian (Siberian Traps). The evidence presented here should alleviate this particular concern.

Supplementary data to this article can be found online at http://dx.doi.org/10.1016/j.palaeo.2012.06.029.

Acknowledgments

We thank Dr. Isern and Dr. Borg of NSF Polar Programs for grants OPP-0739541 (PI Kirschvink) and OPP-0739432 (PI's Ward and Steig). We also acknowledge funding from PICTO 36315 and 0114 ANPCyT-DNA (Olivero). We thank two anonymous reviewers for their comments which improved the manuscript. We would also like to thank David J. Smith, Alvar Sobral, Tomás Wagener, Melissa Rider, Stian Alesandrini, John Evans, Dave Barbeau, Andrew Schauer, and Ron Sletten for assistance in the field and laboratory. Magnetostratigraphic data for this paper are available in the supplemental online material and at the MagIC portal, and the isotopic data is available as a supplemental data set and on the UW Isolab website (http://depts.washington.edu/isolab/data/). Fossil material is held at the University of Washington's Burke Museum of Natural History.

References

Altman, D.G., Bland, J.M., 2005. Standard deviations and standard errors. British Medical Journal 331, 903.
Alvarez, W., 2003. Comparing the evidence relevant to impact and flood basalt at times of major mass extinctions. Astrobiology 3, 153–161.
Alvarez, W., Arthur, M.A., Fischer, A.G., Lowrie, W., Napoleone, G., Silva, I.P., Roggenthen, W.M., 1977. Upper Cretaceous–Paleocene magnetic stratigraphy at Gubbio, Italy V. Type section for the Late Cretaceous–Paleocene geomagnetic reversal time scale. Geological Society of America Bulletin 88, 383.
Alvarez, L.W., Alvarez, W., Asaro, F., Michel, H.V., 1980. Extraterrestrial cause for the Cretaceous–Tertiary extinction. Science 208, 1095.
Archibald, J.D., Clemens, W.A., Padian, K., Rowe, T., Macleod, N., Barrett, P.M., Gale, A., Holroyd, P., Sues, H.D., Arens, N.C., Horner, J.R., Wilson, G.P., Goodwin, M.B., Brochu, C.A., Lofgren, D.L., Hurlbert, S.H., Hartman, J.H., Ebreth, D.A., Wignall, P.B., Currie, P.J., Weil, A., Prasad, G.V.R., Dingus, L., Courtillot, V., Milner, A., Milner, A., Bajpai, S., Ward, D.J., Sahni, A., 2010. Cretaceous extinctions: multiple causes. Science 328, 973.
Arens, N.C., West, I.D., 2008. Press-pulse: a general theory of mass extinction? Paleobiology 34, 456–471.
Barrera, E., 1994. Global environmental changes preceding the Cretaceous–Tertiary boundary: Early–late Maastrichtian transition. Geology 22, 877.
Barrera, E., Savin, S.M., 1999. Evolution of late Campanian–Maastrichtian marine climates and oceans. Geological Society of America Special Paper 332, 245–282.
Barrera, E., Huber, B.T., Savin, S.M., Webb, P.-N., 1987. Antarctic marine temperatures: Late Campanian through Early Paleocene. Paleoceanography 2, 21–47.
Becker, L., Poreda, R.J., Hunt, A.G., Bunch, T.E., Rampino, M., 2001. Impact event at the Permian–Triassic Boundary: evidence from extraterrestrial noble gases in fullerenes. Science 291, 1530–1533.
Bowman, V.C., Francis, J.E., Riding, J.B., Hunter, S.J., Haywood, A.M., 2012. A latest Cretaceous to earliest Paleogene dinoflagellate cyst zonation of Antarctica, and implications for phytoprovincialism in the high southern latitudes. Review of Palaeobotany and Palynology 171, 40–56.
Brand, U., Morrison, J.O., 1987. Paleoscene# 6. Biogeochemistry of fossil marine invertebrates. Geoscience Canada 14.
Chenet, A.L., Courtillot, V., Fluteau, F., Gérard, M., Quidelleur, X., Khadri, S.F.R., Subbarao, K.V., Thordarson, T., 2009. Determination of rapid Deccan eruptions across the Cretaceous–Tertiary boundary using paleomagnetic secular variation: 2. Constraints from analysis of eight new sections and synthesis for a 3500-m-thick composite section. Journal of Geophysical Research 114, B06103.
Cisowski, S., 1981. Interacting vs. non-interacting single domain behavior in natural and synthetic samples. Physics of the Earth and Planetary Interiors 26, 56–62.
Courtillot, V.E., Fluteau, F., 2010. Cretacous extinctions: the volcanic hypothesis. Science 328, 973–974.
Courtillot, V.E., Renne, P.R., 2003. On the ages of flood basalt events. Geodynamics 335, 113–140.
Crame, J.A., Francis, J.E., Cantrill, D.J., Pirrie, D., 2004. Maastrichtian stratigraphy of Antarctica. Cretaceous Research 25, 411–423.
Ditchfield, P.W., Marshall, J.D., Pirrie, F., 1994. High latitude palaeotemperature variation: new data from the Tithonian to Eocene of James Ross Island, Antarctica. Palaeogeography, Palaeoclimatology, Palaeoecology 107, 79–101.
Dunlop, D.J., Ozdemir, O., 1997. Rock Magnetism. Cambridge University Press.
Dutton, A., Huber, B.T., Lohmann, K.C., Zinsmeister, W.J., 2007. High-resolution stable isotope profiles of a dimitobelid belemnite: implications for paleodepth habitat and Late Maastrichtian climate seasonality. Palaios 22, 642.
Elliot, D.H., Askin, R.A., Kyte, F.T., Zinsmeister, W.J., 1994. Iridium and dinocysts at the Cretaceous–Tertiary boundary on Seymour Island, Antarctica: implications for the KT event. Geology 22, 675.
Elorza, J., Gomez Alday, J.J., Olivero, E.B., 2001. Environmental stress and diagenetic modifications in inoceramids and belemnites from the Upper Cretaceous James Ross basin, Antarctica. Facies 44, 227–242.
Farley, K.A., Ward, P., Garrison, G., Mukhopadhyay, S., 2005. Absence of extraterrestrial ^{3}He in Permian–Triassic age sedimentary rocks. Earth and Planetary Science Letters 240, 265–275.
Filmer, P.E., Kirschvink, J.L., 1989. A paleomagnetic constaint on the Late Cretaceous Paleoposition of Northwestern Baja California, Mexico. Journal of Geophysical Research 94, 7332–7342.
Fisher, R., 1953. Dispersion on a sphere. Proceedings of the Royal Society of London. Series A: Mathematical and Physical Sciences 217, 295.

Fuller, M., Cisowski, S., Hart, M., Haston, R., Schmidtke, E., Jarrard, R., 1988. NRM: IRM(S) demagnetization plots; an aid to the interpretation of natural remanent magnetization. Geophysical Research Letters 15, 518–521.
Gradstein, F.M., Ogg, J.G., Smith, A.G., 2004. A Geologic Time Scale 2004. Cambridge University Press.
Halgedahl, S.L., 1993. Experiments to investigate the origin of anomalously elevated unblocking temperatures. Journal of Geophysical Research 98, 22443–22460.
Hildebrand, A.R., Penfield, G.T., Kring, D.A., Pilkington, M., Camargo, Z.A., Jacobsen, S.B., Boynton, W.V., 1991. Chicxulub Crater: a possible Cretaceous/Tertiary boundary impact crater on the Yucatán Peninsula, Mexico. Geology 19, 867.
Holland, M.M., Bitz, C.M., 2003. Polar amplification of climate change in coupled models. Climate Dynamics 21, 221–232.
Jay, A.E., Niocaill, C.M., Widdowson, M., Self, S., Turner, W., 2009. New palaeomagnetic data from the Mahabaleshwar Plateau, Deccan Flood Basalt Province, India: implications for the volcanostratigraphic architecture of continental flood basalt provinces. Journal of the Geological Society 166, 13–24.
Kim, S.T., O'Neil, J.R., 1997. Equilibrium and nonequilibrium oxygen isotope effects in synthetic carbonates. Geochimica et Cosmochimica Acta 61, 3461–3475.
Kim, S.T., Mucci, A., Taylor, B.E., 2007a. Phosphoric acid fractionation factors for calcite and aragonite between 25 and 75 °C: revisited. Chemical Geology 246, 135–146.
Kim, S.T., Oneil, J., Hillairemarcel, C., Mucci, A., 2007b. Oxygen isotope fractionation between synthetic aragonite and water: influence of temperature and Mg^{2+} concentration. Geochimica et Cosmochimica Acta 71, 4704–4715.
Kirschvink, J.L., 1980. The least-squares line and plane and the analysis of palaeomagnetic data. Geophysical Journal of the Royal Astronomical Society 62, 699–718.
Kirschvink, J.L., Kopp, R.E., Raub, T.D., Baumgartner, C., Holt, J.W., 2008. Rapid, precise, and high-sensitivity acquisition of paleomagnetic and rock-magnetic data: development of a low-noise automatic sample changing system for superconducting rock magnetometers. Geochemistry, Geophysics, Geosystems 9.
Kobayashi, A., Kirschvink, J.L., Nash, C.Z., Kopp, R.E., Sauer, D.A., Bertani, L.E., Voorhout, W.F., Taguchi, T., 2006. Experimental observation of magnetosome chain collapse in magnetotactic bacteria: sedimentological, paleomagnetic, and evolutionary implications. Earth and Planetary Science Letters 245, 538–550.
Kump, L.R., Pavlov, A., Arthur, M.A., 2005. Massive release of hydrogen sulfide to the surface ocean and atmosphere during intervals of oceanic anoxia. Geol 33, 397.
Li, L., Keller, G., 1998. Abrupt deep-sea warming at the end of the Cretaceous. Geology 26, 995.
Lowenstam, H.A., Weiner, S., 1989. On Biomineralization. Oxford University Press, New York.
Macellari, C.E., 1986. Late Campanian–Maastrichtian ammonite fauna from Seymour Island (Antarctic Peninsula). Memoir (The Paleontological Society) 18, 1–55.
Macellari, C.E., 1987. Progressive endemism in the Late Cretaceous ammonite family Kossmaticeratidea and the breakup of Gondwanaland. Gondwana Six: Stratigraphy, Sedimentolody, and Paleontology 85–92.
Macellari, C.E., 1988. Stratigraphy, sedimentology, and paleoecology of Upper Cretaceous/Paleocene shelf-deltaic sediments of Seymour Island. Geology and paleontology of Seymour Island, Antarctic Peninsula 169, 25–54.
Manabe, S., Stouffer, R.J., 1980. Sensitivity of a global climate model to an increase of CO_2 concentration in the atmosphere. Journal of Geophysical Research 85, 5529–5554.
Marshall, C.R., 1995. Distinguishing between sudden and gradual extinctions in the fossil record: predicting the position of the Cretaceous–Tertiary iridium anomaly using the ammonite fossil record on Seymour Island, Antarctica. Geology 23, 731.
McArthur, J.M., Crame, J.A., Thirlwall, M.F., 2000. Definition of Late Cretaceous stage boundaries in Antarctica using strontium isotope stratigraphy. Journal of Geology 108, 623–640.
McFadden, P.L., McElhinny, M.W., 1988. The combined analysis of remagnetization circles and direct observations in palaeomagnetism. Earth and Planetary Science Letters 87, 161–172.
McFadden, P.L., McElhinny, M.W., 1990. Classification of the reversal test in palaeomagnetism. Geophysical Journal International 103, 725–729.
McLaren, D.J., 1985. Mass extinction and iridium anomaly in the Upper Devonian of Western Australia: a commentary. Geology 13, 170.
Morrison, J.O., Brand, U., 1986. Paleoscene# 5. Geochemistry of Recent Marine Invertebrates. Geoscience Canada 13.
Olivero, E.B., 2012. Sedimentary cycles, ammonite diversity and palaeoenvironmental changes in the Upper Cretaceous Marambio Group, Antarctica. Cretaceous Research 34, 348–366.
Olivero, E.B., Medina, F.A., 2000. Patterns of Late Cretaceous ammonite biogeography in southern high latitudes: the family Kossmaticeratidae in Antarctica. Cretaceous Research 21, 269–279.
Olivero, E.B., Ponce, J.J., Marsicano, C.A., Martinioni, D.R., 2007. Depositional settings of the basal López de Bertodano Formation, Maastrichtian, Antarctica. Revista de la Asociación Geológica Argentina 62, 521–529.
Olsen, P.E., Kent, D.V., Sues, H.D., Koeberl, C., Huber, H., Montanari, A., Rainforth, E.C., Fowell, S.J., Szajna, M.J., Hartline, B.W., 2002. Ascent of dinosaurs linked to an iridium anomaly at the Triassic–Jurassic boundary. Science 296, 1305.
Pirrie, D., 1994. Petrography and provenance of the Marambio Group, Vega Island, Antarctica. Antarctic Science 6, 517–527.
Playford, P.E., McLaren, D.J., Orth, C.J., Gilmore, J.S., Goodfellow, W.D., 1984. Iridium anomaly in the Upper Devonian of the Canning Basin, western Australia. Science 226, 437.
Robinson, N., Ravizza, G., Coccioni, R., Peucker-Ehrenbrink, B., Norris, R., 2009. A high-resolution marine $^{187}Os/^{188}Os$ record for the late Maastrichtian: distinguishing the chemical fingerprints of Deccan volcanism and the KP impact event. Earth and Planetary Science Letters 281, 159–168.
Schulte, P., Alegret, L., Arenillas, I., Arz, J.A., Barton, P.J., Bown, P.R., Bralower, T.J., Christeson, G.L., Claeys, P., Cockell, C.S., Collins, G.S., Deutsch, A., Goldin, T.J., Goto, K., Grajales-Nishimura, J.M., Grieve, R.A.F., Gulick, S.P.S., Johnson, K.R., Kiessling, W., Koeberl, C., Kring, D.A., MacLeod, K.G., Matsui, T., Melosh, J., Montanari, A., Morgan, J.V., Neal, C.R., Nichols, D.J., Norris, R.D., Pierazzo, E., Ravizza, G., Rebolledo-Vieyra, M., Reimold, W.U., Robin, E., Salge, T., Speijer, R.P., Sweet, A.R., Urrutia-Fucugauchi, J., Vajda, V., Whalen, M.T., Willumsen, P.S., 2010. The Chicxulub asteroid impact and mass extinction at the Cretaceous–Paleogene boundary. Science 327, 1214–1218.
Shackleton, N.J., Kennett, J.P., 1975. Late Cenozoic oxygen and carbon isotopic changes at DSPDP Site 284: implications for glacial history of the Northern Hemisphere and Antarctica. Initial Reports of the Deep Sea Drilling Project, 29, pp. 801–807.
Tanner, L.H., Kyte, F.T., Walker, A.E., 2008. Multiple Ir anomalies in uppermost Triassic to Jurassic-age strata of the Blomidon Formation, Fundy basin, eastern Canada. Earth and Planetary Science Letters 274, 103–111.
Torsvik, T.H., Müller, R.D., Van der Voo, R., Steinberger, B., Gaina, C., 2008. Global plate motion frames: toward a unified model. Reviews of Geophysics 46.
Van der Voo, R., 1993. Paleomagnetism of the Atlantic, Tethys, and Iapetus oceans. Cambridge University Press.
Wang, S.C., Marshall, C.R., 2004. Improved confidence intervals for estimating the position of a mass extinction boundary. Paleobiology 30, 5–18.
Ward, P.D., Hurtado, J.M., Kirschvink, J.L., Verosub, K.L., 1997. Measurements of the Cretaceous paleolatitude of Vancouver Island: consistent with the Baja–British Columbia hypothesis. Science 277, 1642.
Weiner, S., Dove, P.M., 2003. An overview of biomineralization processes and the problem of the vital effect. Reviews in Mineralogy and Geochemistry 54, 1.
White, R.V., Saunders, A.D., 2005. Volcanism, impact and mass extinctions: incredible or credible coincidences? Lithos 79, 299–316.
Whiteside, J.H., Olsen, P.E., Eglinton, T., Brookfield, M.E., Sambrotto, R.N., 2010. Compound-specific carbon isotopes from Earth's largest flood basalt eruptions directly linked to the end-Triassic mass extinction. Proceedings of the National Academy of Sciences 107, 6721.
Wignall, P.B., 2001. Large igneous provinces and mass extinctions. Earth-Science Reviews 53, 1–33.
Wilf, P., Johnson, K.R., Huber, B.T., 2003. Correlated terrestrial and marine evidence for global climate changes before mass extinction at the Cretaceous–Paleogene boundary. Proceedings of the National Academy of Sciences of the United States of America 100, 599.
Zinsmeister, W.J., Feldmann, R.M., Woodburne, M.O., Elliot, D.H., 1989. Latest Cretaceous/earliest Tertiary transition on Seymour Island, Antarctica. Journal of Paleontology 63, 731–738.